Supporting Information For:

Connecting Crystal Structure with Chromophore Design to Rationalise Fluorescence in the Solid State

Michael Dommett, Miguel Rivera, Matthew Tyler Hollis-Smith, Rachel Crespo-Otero*

School of Biological and Chemical Sciences, Materials Research Institute,

Queen Mary University of London, Mile End Road, London E1 4NS, UK

E-mail: r.crespo-otero@qmul.ac.uk

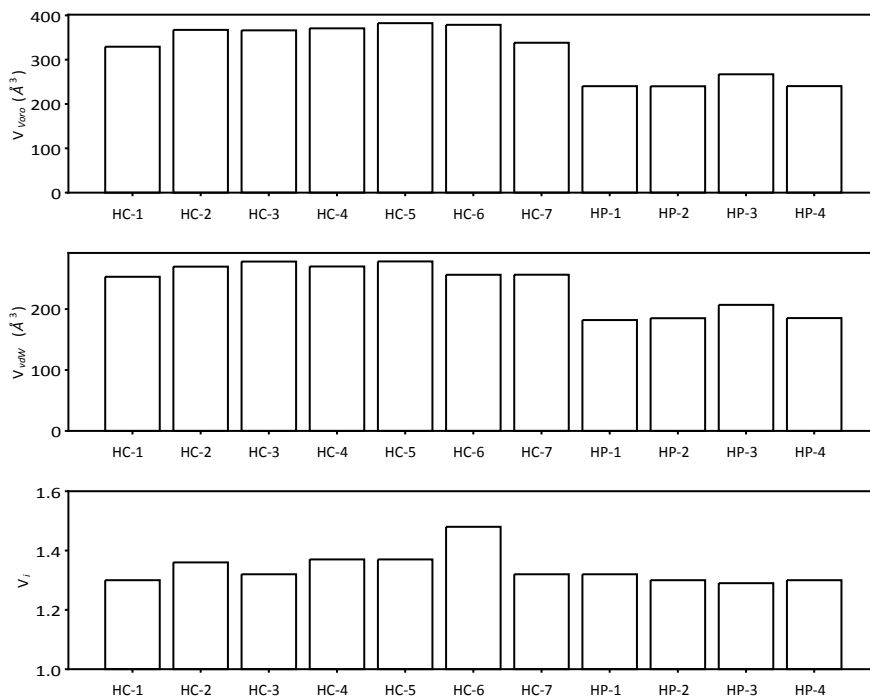## Contents

S1 Crystal Packing Properties

Figure S1: Voronoi volumes (V_{Voro}), van der Waals volumes (V_{vdW}) and the index ($V_i = V_{Voro}/V_{vdW}$)
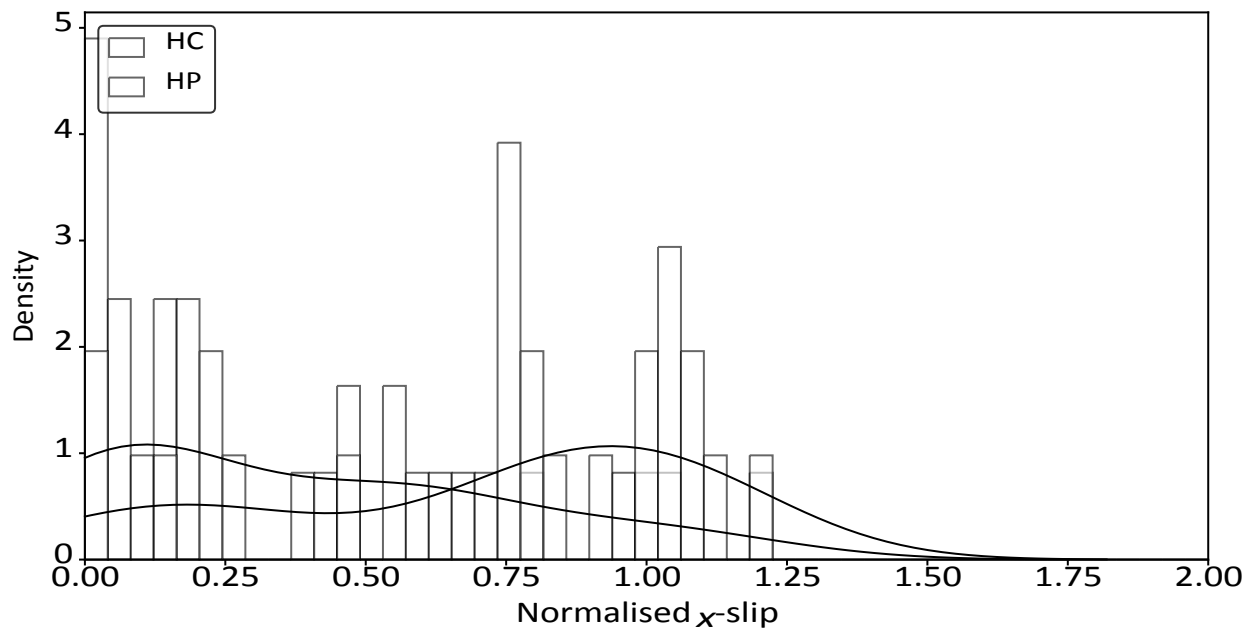

Figure S2: The density of slip distances for each molecular dimer in the *x*-plane (long axis) for cofacial dimers. The slip is normalised by the length of the long axis *x* for each molecule, such that slip is molecule independent.
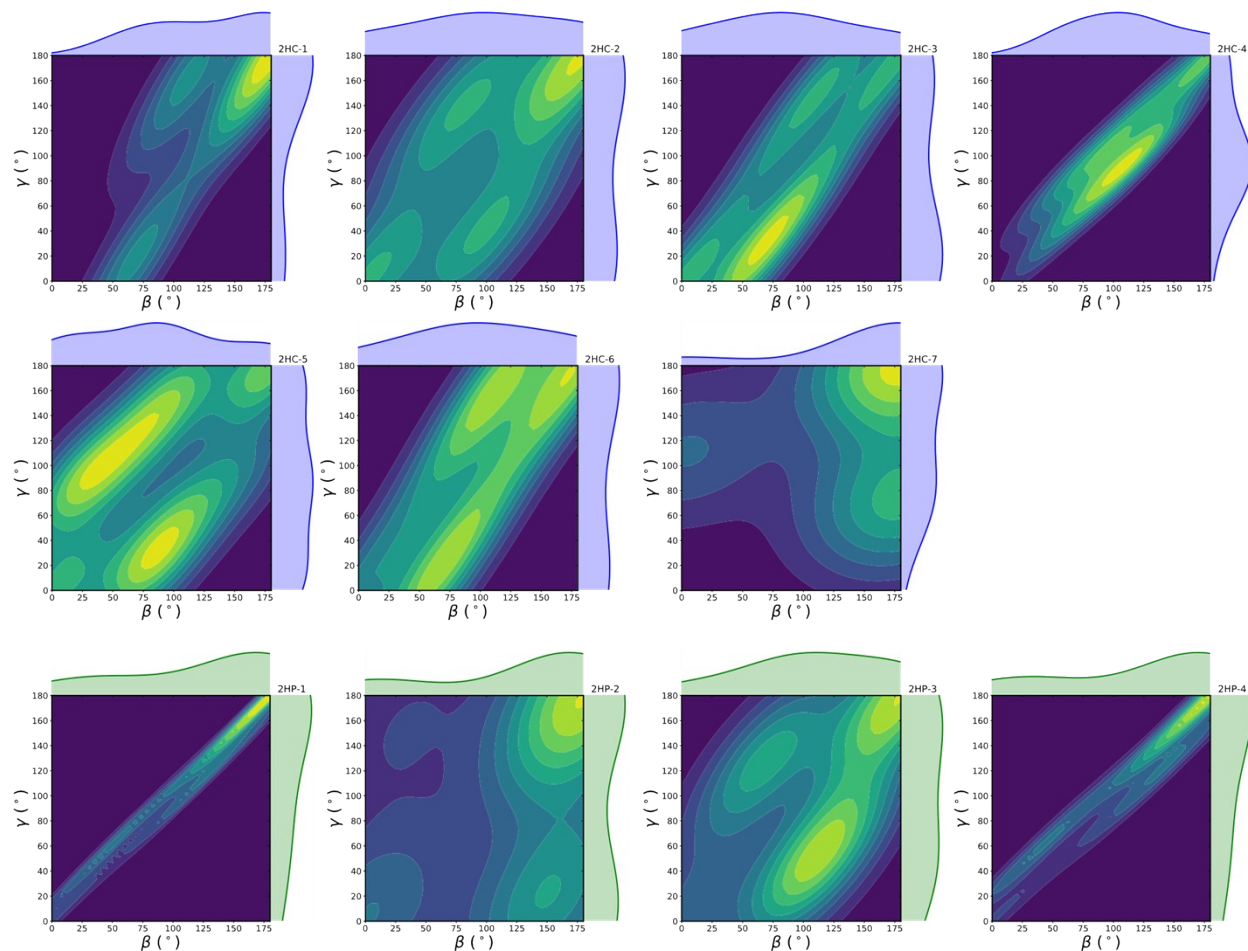
Figure S3: Probability density map of β and γ angles for each of the systems understudy
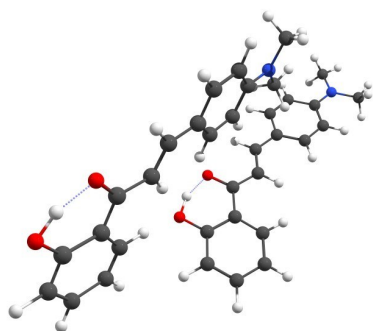
Table S1: Dimer classification definitions

	α Condition	β Condition	γ Condition
Herringbone	$\alpha \leq 60°$	$45° \leq \beta \leq 135°$	$\gamma \leq 45° \vee (135° \leq \gamma \leq 225°)$
Parallel T	$\alpha \leq 60°$	$\beta \leq 45° \vee (135° \leq \beta \leq 225)$	$45° \leq \gamma \leq 135°$
Perpendicular T	$\alpha \leq 60°$	$45° \leq \beta \leq 135°$	$45° \leq \gamma \leq 135°$
CoFacial	$\alpha \leq 60°$	$\beta \leq 45° \vee (135° \leq \beta \leq 225)$	$\gamma \leq 45° \vee (135° \leq \gamma \leq 225°)$

Table S2: Dimer classifications in each molecular crystal for $\alpha \leq 60°$. Significant increase in HC5 dimers due to rotational flexibility of the methoxy group.

System	Herringbone	Parallel-T	Perpendicular-T	CoFacial
HC1	3	0	0	1
HC2	4	0	0	0
HC3	3	0	0	0
HC4	1	0	4	0
HC5	9	6	4	3
HC6	3	0	0	1
HC7	0	3	0	0

HP1	0	0	3	1
HP2	0	0	0	2
HP3	0	0	2	1
HP4	0	3	0	1

Herringbone Parallel   Herringbone Antiparallel
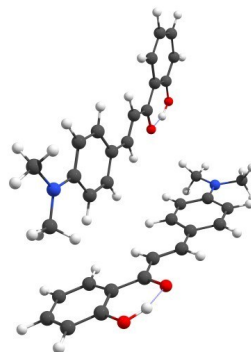
α: 56° β: 68° γ: 18°   α: 18° β: 112° γ: 162°
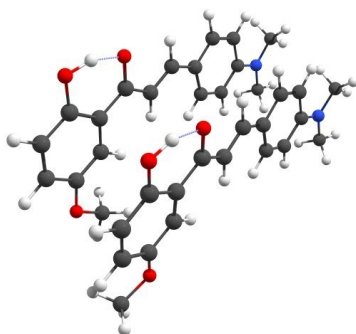
CoFacial Parallel   CoFacial-Antiparallel

α: 16° β: 5° γ: 3°   α: 11° β: 180° γ: 180°
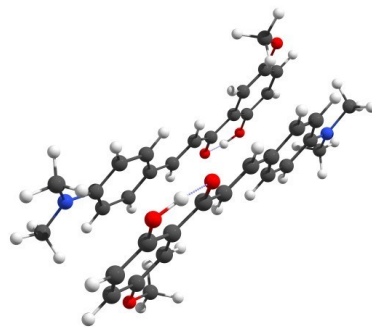
Parallel T   Perpendicular T
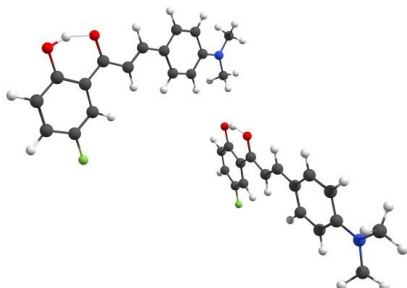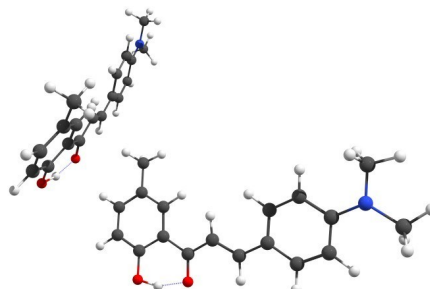
α: 41° β: 3° γ: 111°   α: 22° β: 58° γ: 80°

Figure S4: Example dimer packing modes and associated α, β and γ angles in **HC1**, **HC5**, and **HP1.**

S2   Huang-Rhys Factors

Normal modes can be correlated between different electronic states using the the Duschinsky rotation matrix, yielding the Huang-Rhys factors S between the electronic states for each frequency ω

$$S_j = \frac{\omega_j D_j^2}{2\hbar} \tag{S1}$$

where D_j is the displacement of mode j between the equilibrium geometry in the considered electronic states. Summation of each Huang-Rhys factor yields the normal mode reorganisation energy for the system

$$\lambda_{NM} = \sum_{j=1}^{3N-6} h\bar{\omega}_j S_j \tag{S2}$$

Where we have deleted the rotational and translational degrees of freedom. Whilst these modes would be useful to quantify in crystal, the employed cluster model means that the vibrational analysis calculation is *de facto* in vacuum with added Coulomb corrections from the electrostatic embedding of the QM/MM.

In this section, we calculate the HR factors for **HC1**, **HC5**, and **HP1**.

The Huang-Rhys (HR) factors in vacuum and molecular crystals were calculated for **HC1**, **HC5**, and **HP1**. In vacuum, ground and excited states were optimised at (TD-)ωB97X-d/631G(d) level. In the molecular crystal, a cluster model consisting of a central chromophore and all molecules within a 7˚A, taken from the optimised unit cell for each system (see main text for unit cell optimisation details). Ground and excited states were optimised at ONIOM((TD-)ωB97X-d/6-31G(d):AMBER) level, and frequencies were calculated at (TD)ωB97X-d/6-31G(d) level using point charge embedding. The DUSHIN program was used to calculate the Huang-Rhys factors and the associated reorganisation energies (λ_{NM}).

Figures S5-S7 show the Huang-Rhys (HR) factors in vacuum and solid state for **HC1**, **HC5** and **HP1**. The different y-axis scales for the Huang-Rhys factors between plots should be noted. Each system is discussed in turn below.

Figure S5: Huang-Rhys factors associated with each normal mode calculated *via* the Duschinsky rotation matrix between the E* and S_0, and K* and S_0 electronic states for **HC1**. Frequencies 0-500 cm^{-1} in the solid state are shown in the inset.

Figure S6: Huang-Rhys factors associated with each normal mode calculated *via* the Duschinsky rotation matrix between K* and S_0 electronic states for **HC5**. Frequencies 0-500 cm^{-1} in the solid state are shown in the inset.
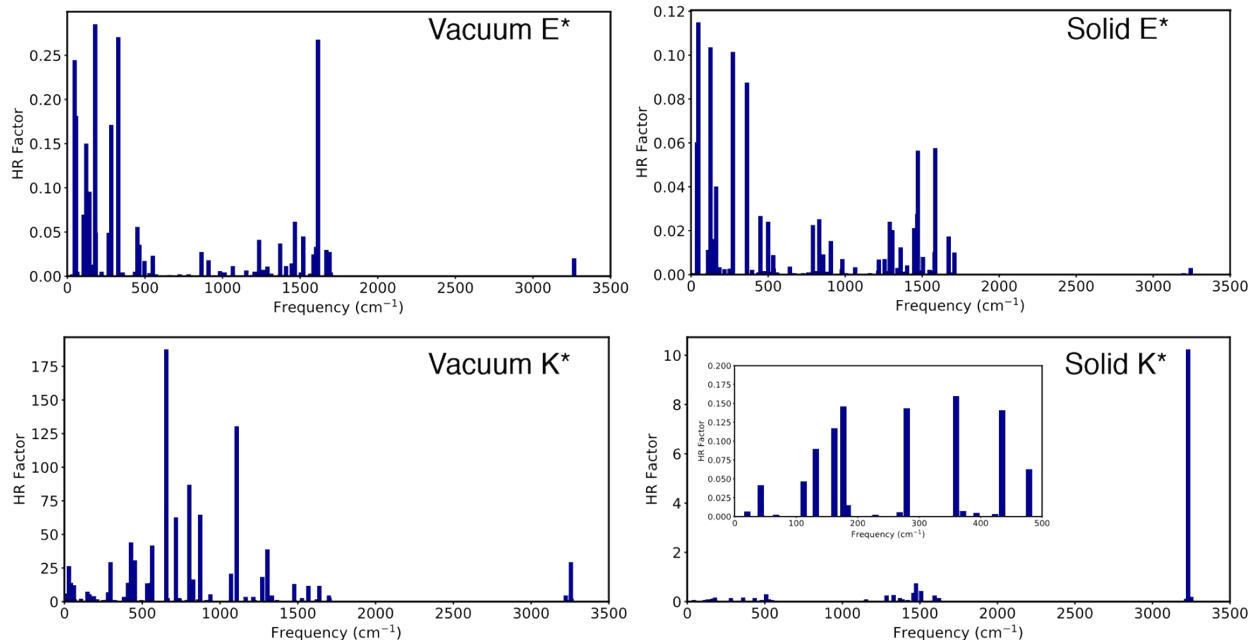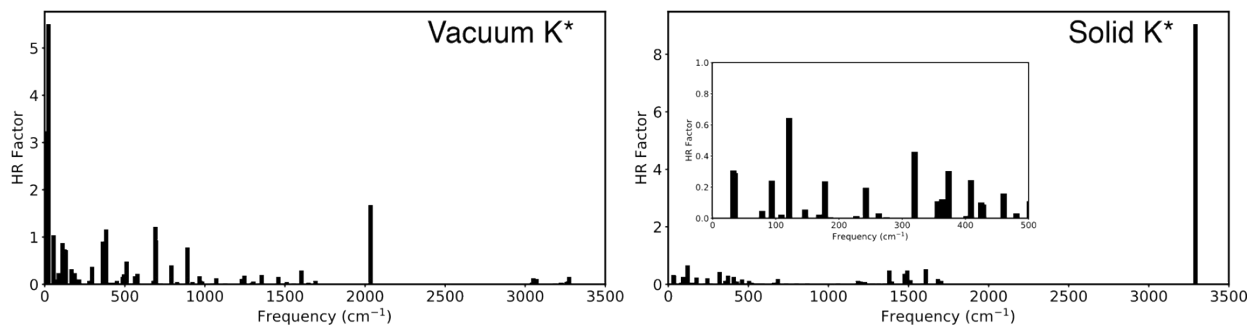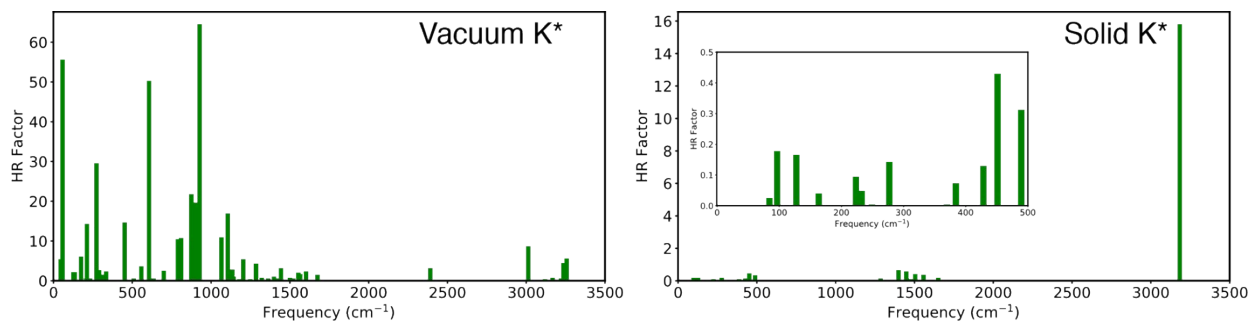
Figure S7: Huang-Rhys factors associated with each normal mode calculated *via* the Duschinsky rotation matrix between K* and S_0 electronic states for **HP1**. Frequencies 0-500 cm^{-1} in the solid state are shown in the inset.

For **HC1** in vacuum (Figure S5, left), the geometric similarity between the planar E* excited state minimum and the ground state equilibrium geometry yields negligible HR factors. This leads to λ_{NM} of 0.08 eV, which underestimates the λ_A of 0.36. For K*, the PES in vacuum is highly anharmonic, and intramolecular rotation leads to a highly distorted geometry with respect to the ground state. As a consequence, the HR factors are extremely large and the harmonic approximation is non-applicable for determining the reorganisaiton energy, as shown by a value of 99 eV (λ_A=3.64 eV). Moving to the molecular crystal (Figure S5, right), in E* the HR factors are of similar magnitude as in vacuum but in K* they are markedly reduced and suppressed to fractional values. The largest K* HR factor is the O-H stretching mode, since the geometry remains planar and has the largest displacement between S_0 and S_1 as it is the ESIPT coordinate. The K* λ_{NM} is 4.67 eV, with λ_A=0.59 eV.

In **HC5** there is no stable E* minimum in either vacuum or the solid state for the monomer chromophore. In vacuum, the HR factors are much less than in **HC1** due to the rotation angle at the minimum being less distorted. The molecule is more planar and is closer in structure and vibrational signature. At larger rotation angles the MECI is reached (see Section S6). HR factors are reduced in the solid state, in particular for the rotational modes, but with the O-H stretch HR factor increasing.

For **HP1**, large reorganisation energies, and correspondingly large HR-factors, are associated with low-frequency rotational modes. Indeed, such is the displacement between

7

modes in the ground and excited states, the total reorganisation energy is 41 eV, whereas the adiabatic value 3.89 eV. As such, the harmonic approximation is invalid here due to the excited state potential energy surface anharmonicity. In the solid state, the normal modes associated with rotation are significantly reduced, whilst the largest HR factor is associated with the stretching of the phenol oxygen. This is to be expected, since it is along this coordinate that ESIPT occurs, and hence is has the largest HR-factor. In solid state, λ_{NM} is 2.19 eV, compared with λ_A of 1.24 eV.

In the case of the **HC** and **HP** systems, the AIE behaviour can not be directly attributed to the reduction of the HR factors in the solid state compared to vacuum. Such is the complexity of the PES, where ESIPT and rotation occur in the excited state (in vacuum), the surfaces are highly anharmonic and the validity of the HR scheme via Duschinsky is not clear. As such, it is not the focus of our investigation into the AIE behaviour of these systems.

Table S3: Reorganisation energies (eV) in the adiabatic regime for each system in the enol (where located) and keto minima

System	E*	K*
HC1	0.233	0.786
HC2	0.246	0.804
HC3	0.249	0.668
HC4	0.250	0.935
HC5	-	0.978
HC6	0.210	0.533
HC7	0.213	0.649
HP1	-	1.238
HP2	-	1.059
HP3	-	1.120
HP4	-	1.204

S3   Electronic excitations
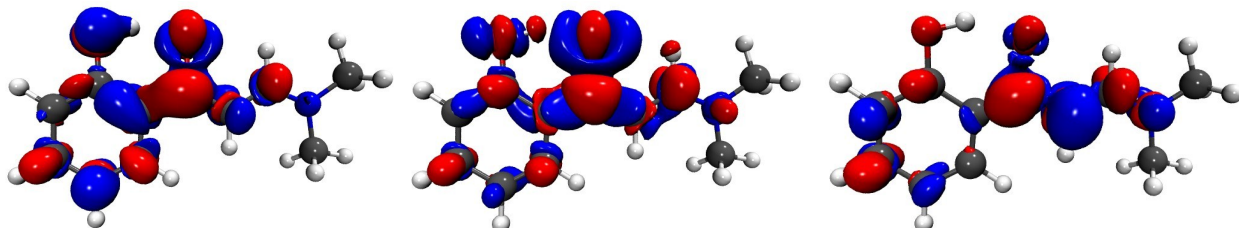
S₁   S₂   S₃

Figure S8: Electron density difference maps for the first three excitations of **HP1**. Blue regions represent electron density loss from the ground state and red represent electron density gain in the excited state, with isovalue of 0.002. Calculated at TD-ωB97X-D/6311++G(d,p) in vacuum.

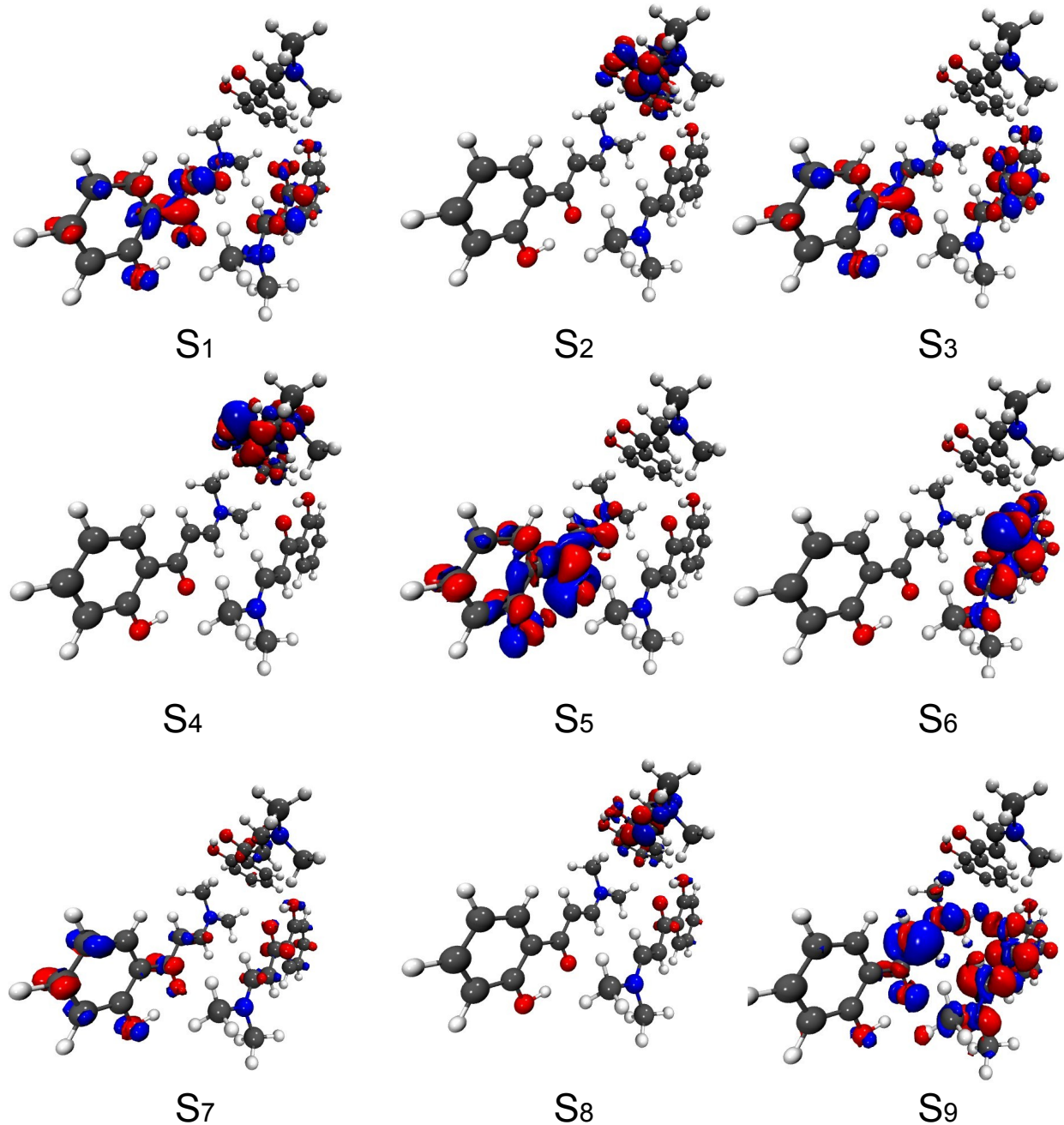Figure S9: Electron density difference maps for the first nine excited state of the **HP1** trimer. The same colour scheme is used as in Figure S8

S4 Exciton Coupling

S4.1 Evaluation

In this work, we employ different methods of computing the exciton coupling between monomers of the crystal. The Coulomb contribution to the coupling J_{ij}^q can be calculated using atom-centred transition charges q,

$$J_{ij}^q = \sum_a^{N_i} \sum_b^{N_j} \frac{q_a q_b}{|\boldsymbol{R}_a^i - \boldsymbol{R}_b^j|}$$

(S3)

where pairwaise contribution of atom a on monomer i and atom b on monomer j is calculated.[1]

For a more complete evaluation of J_{ij}, which also includes non-Coulombic effects, the exciton coupling can be calculated using Troisi's diabatisation scheme based on the orthogonal transformation of adiabatic states to diabatic states via matrix **C**[2,3]

$$\mathbf{H}_D = \mathbf{CH}_A\mathbf{C}†$$

(S4)

$$\mathbf{H}^D = \begin{pmatrix} E_{iD} & J_{ij} \\ J_{ij} & E_{jD} \end{pmatrix} \begin{pmatrix} C_{11} & C_{12} \\ C_{21} & C_{22} \end{pmatrix} \begin{pmatrix} E_{iA} & 0 \\ 0 & E_{jA} \end{pmatrix} \begin{pmatrix} C_{1} & C_{21} \\ C_{12} & C_{22} \end{pmatrix}$$

(S5)

$\mathbf{H}^A$ is the diagonal Hamiltonian of the S_1 and S_2 excitation energies of the dimer and the exciton coupling J_{ij} is in the off-diagonal terms in the diabatic 2x2 Hamiltonian matrix $\mathbf{H}^D$. **C** is computed by singular value decomposition to transform the transition dipole moments of the first two excited states of the dimer and so as to best match the transition dipole moments of the first excited state of the two isolated monomers. In this work we extend Troisi's diabatisation method to asses the effect of a third monomer k on the exciton coupling. In a trimer chromophore, $\mathbf{H}^D$ becomes a 3x3 matrix

$$\begin{pmatrix} E_{iD} & J_{ij} & J_{ik} \\ J_{ji} & E_{jD} & J_{jk} \end{pmatrix} = \begin{pmatrix} C_{11} & C_{12} & C_{13} \\ C_{21} & C_{22} & C_{23} \end{pmatrix} \begin{pmatrix} E_{iA} & 0 & 0 \\ 0 & E_{jA} & 0 \\ 0 & 0 \end{pmatrix} \begin{pmatrix} C_{11} & C_{13} \\ C_{12} & C_{23} \\ C_{21} & C_{22} \\ C_{32} \end{pmatrix}$$

(S6)

$$\begin{pmatrix} \square & & \square\ \square & & \square\square & & \square\square & & C_{33} \\ J_{ki}\,J_{kj}\,E_{kD} & & C_{31}\,C_{32}\,C_{33} & & 0 & & E_{kA}\,C_{31} & \end{pmatrix}$$

where the coupling J_{ij} **between monomers** *i* **and** *j* **incorporates the effect of monomer** *k*, **which can quantified through comparison of the dimeric and trimeric** J_{ij}.

S4.2 Results in Trimers

The exciton coupling in trimers was calculated for **HC1, HC5**, and **HP1**. The results are given in Table S4, and shown schematically in Figure S9, where the couplings obtained in a dimer scheme are compared to those obtained when an additional molecule is included.

It is found that the addition of a third molecule has only a small effect on the dimer coupling in **HP1** and **HC1**, where the increased coupling in one dimer is compensated for by the decreased coupling in the other dimer, with difference of less that 0.02 eV. The largest effect is seen in **HC5** due to the cofacial packing of the trimer system, where the central monomer is sandwiched by two cofacially stacked monomers, one parallel and one antiparallel. In this system, the parallel dimer ($\gamma = 0$) has its coupling increased by 0.04 eV with the addition of the third molecule, which is aligned antiparallel ($\gamma = 180$). Conversely, the antiparallel coupling is reduced by 0.07 eV due to the parallel stacked monomer.

Table S4: Exciton coupling comparison for dimer and trimer in HC1, HC5, and HP1

System	Dimer Coupling (eV)	Trimer Coupling (eV)
	0.108	0.090
	0.108	0.125
HC1		
	0.061 0.063	0.061 0.052
HC5		
	0.116 0.157	0.142 0.085

12

(0.108)
0.125

(0.108)
0.090

0.0040.

(0.142)
0.085

(0.004)
0.001

(0.005)
0.014

(0.061)
0.052

(0.061)
0.063

HP1

(0.056)

0.056
0.005
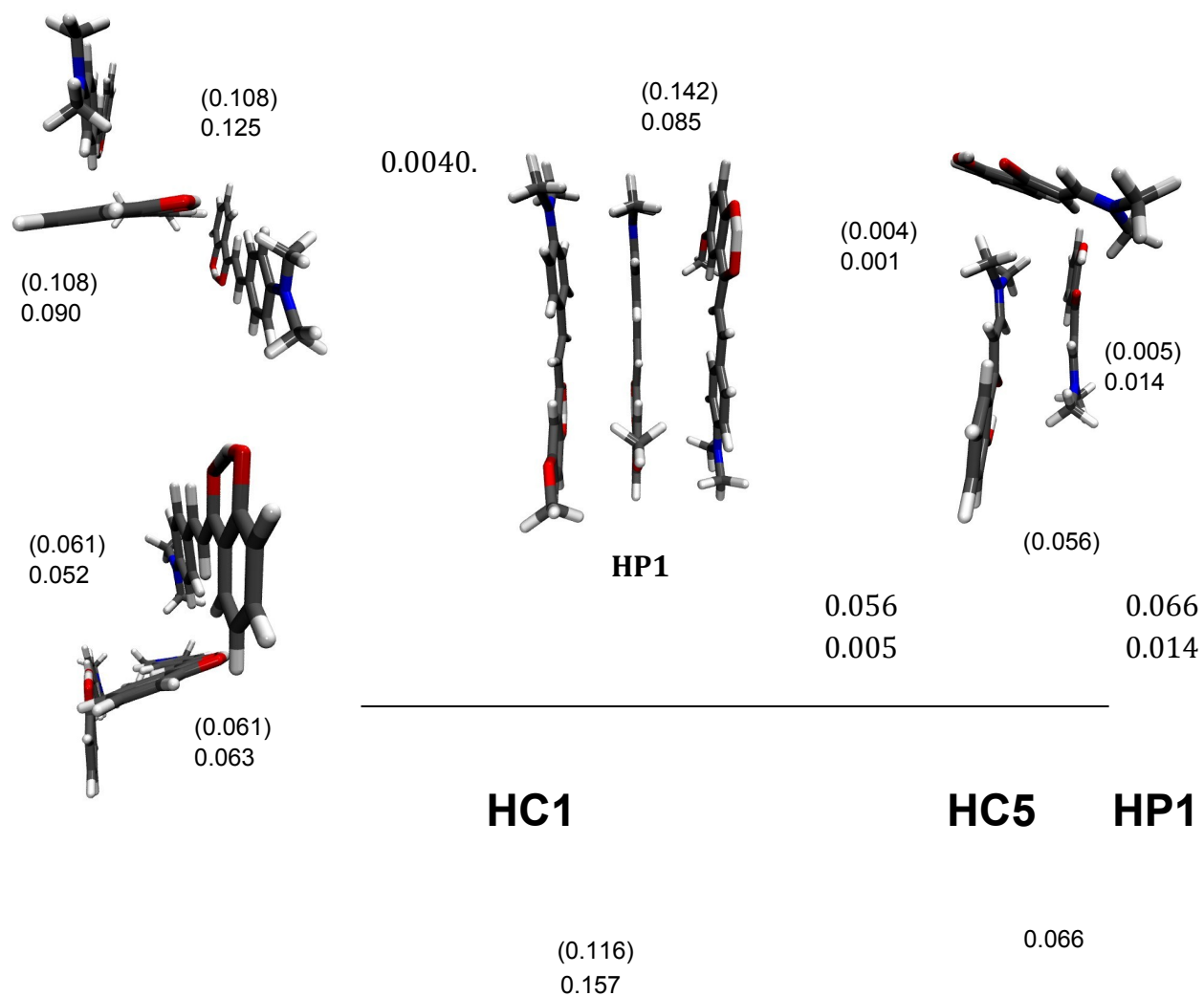
0.066
0.014

HC1

HC5   HP1

(0.116)
0.157

0.066

Figure S10: Schematic of the trimer motifs extracted from unit cells of **HC1**, **HC5** and **HP1**. Exciton couplings for dimer pairs (shown in brackets) and then for the full trimer are shown. Calculated at ωB97X-D/6-311++G(d,p) level of theory using the diabatisation described in the main text.
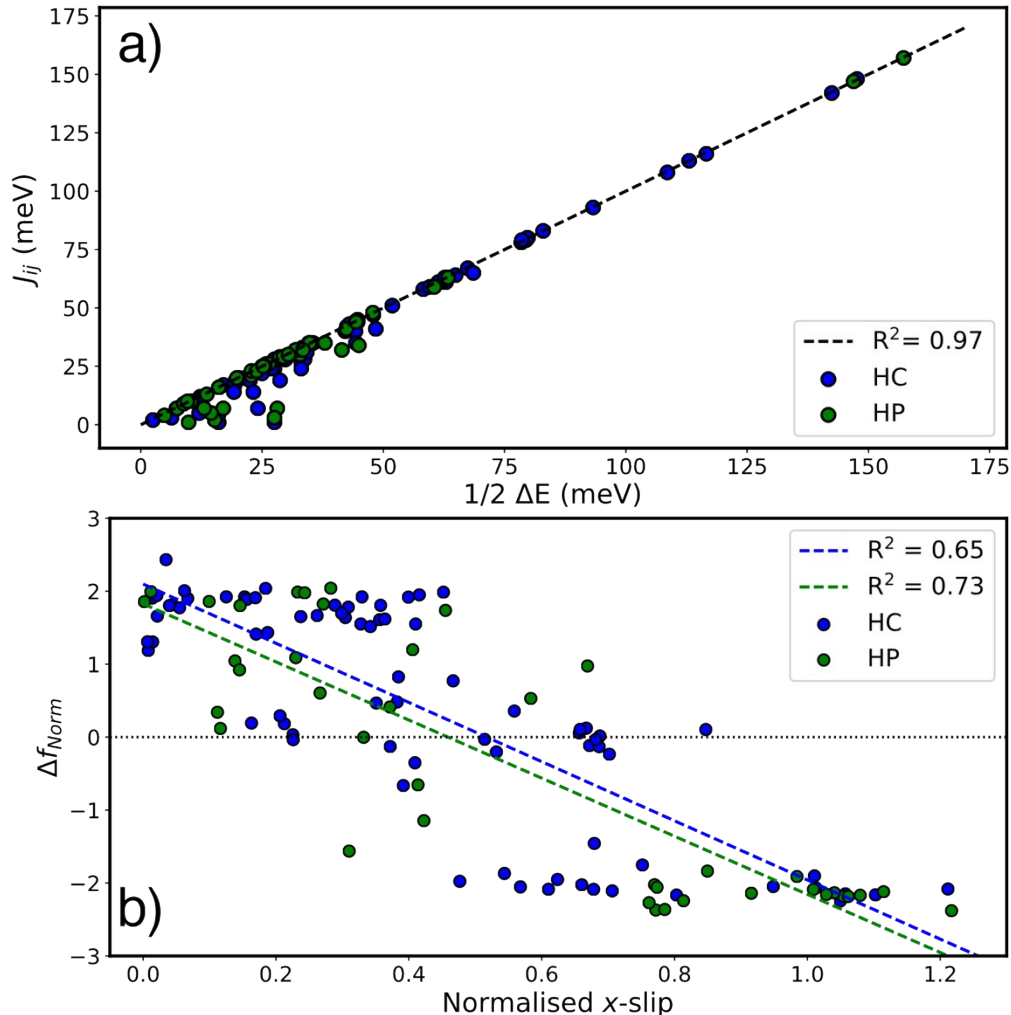
S5   H- and J-Aggregates

Figure S11: Panel a), top; Correlation between the energy splitting of the dimer states and the diabatic exciton coupling. Panel b), bottom; Linear regression of the x-slip against the difference in oscillator strength between the S_2 and S_1 states in dimers. The definition of Δf_{Norm} is given in Equation S7

As shown in Figure S11a, the coupling J correlates linearly with half of the energy splitting for the S_1 and S_2 states of the dimer. The energy splitting is perhaps the simplest way to obtain the exciton coupling in the Kasha regime, although it is more computationally costly than using atomic-centred transition charges, or the PDA approximation, since the supermolecular calculation must be done rather than one monomer calculation. At small intermolecular distances (<4˚A), these computationally efficient metrics can underestimate

14

the couplings due to them only considering the Coulomb interaction.[1] The linear correlation here shows that the general Kasha interpretation of the coupling applies here and that the diabatisation method to obtain the couplings reproduces the supramolecular coupling.

Table S5: Dimer types located for each molecular crystal. Significant increase in HC5 dimers due to rotational flexibility of the methoxy group

System	H-aggregates	J-aggregates	Total
HC1	4	4	8
HC2	5	4	9
HC3	4	5	9
HC4	7	2	9
HC5	19	10	29
HC6	4	3	7
HC7	6	0	6
HP1	5	5	10
HP2	5	6	11
HP3	4	5	9
HP4	5	5	10

In the Kasha model, for a perfectly stacked dimer with no x-slip, the oscillator strength of the S_2 state should be double that of the monomer state. Figure S11b shows the relationship between the x-slip in the dimers and the oscillator strength, namely the difference in oscillator strength between the S_2 and S_1 states in the dimer, normalised by the corresponding mononomer oscillator strength

$$\Delta f_{Norm} = \frac{f_{S_2}^{dimer} - f_{S_1}^{dimer}}{f_{S_1}^{monomer}}. \tag{S7}$$

These systems generally fit the Kasha model, as when the x-slip is zero, the line of best fit predicts an enhanced S_2 intensity of 2.10 for the **HC**s and 1.83 for the **HP**s. With increasing x-slip, the difference in oscillator strength between the two states decreases until the inversion to J-aggregates is witnessed ($f_{S_1} > f_{S_2}$). For the **HC**s this occurs at a x-slip of 52% and at 46% for the **HC**s. However, there is some significant noise in the model, which is understandable given its simplicity and the complex electronic structure of the dimer. The

largest group of outliers are cofacially stacked dimers, where a larger shift is seen at lower slip distances due to the minimal x-slip and archetypal stacking.[4]
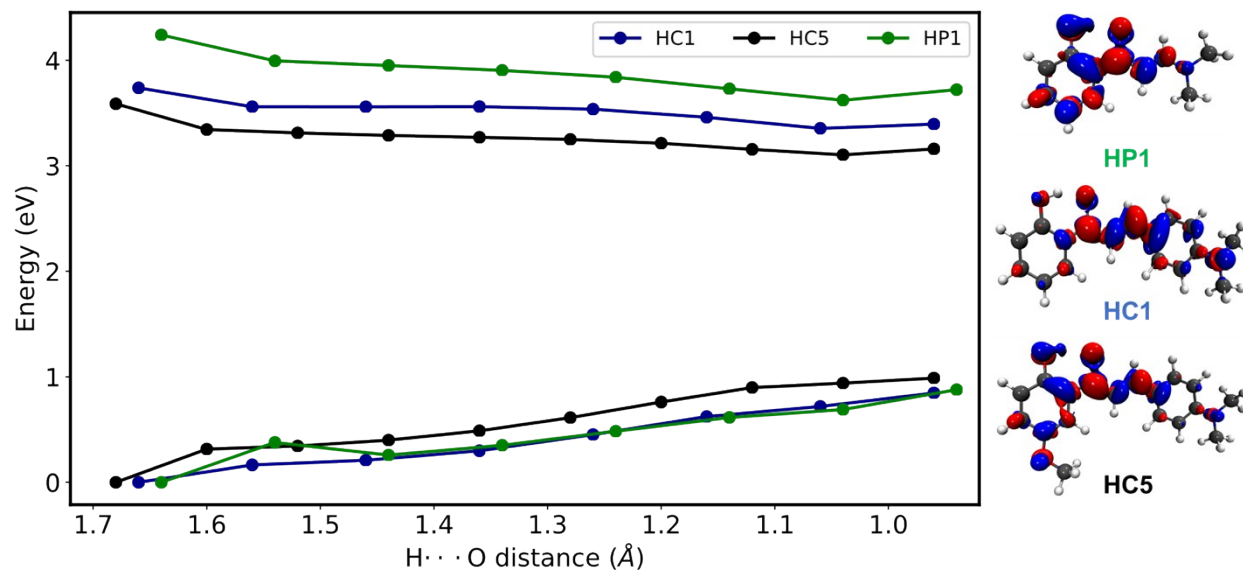
S6 Bias for ESIPT

Figure S12: Relaxed geometry scan of the phenol hydrogen to carbonyl oxygen distance for **HC1**, **HC5** and **HP1**, calculated at TD-ωB87X-D/6-31G(d). Electron density difference maps are also shown, with same labelling as for Figure S8.
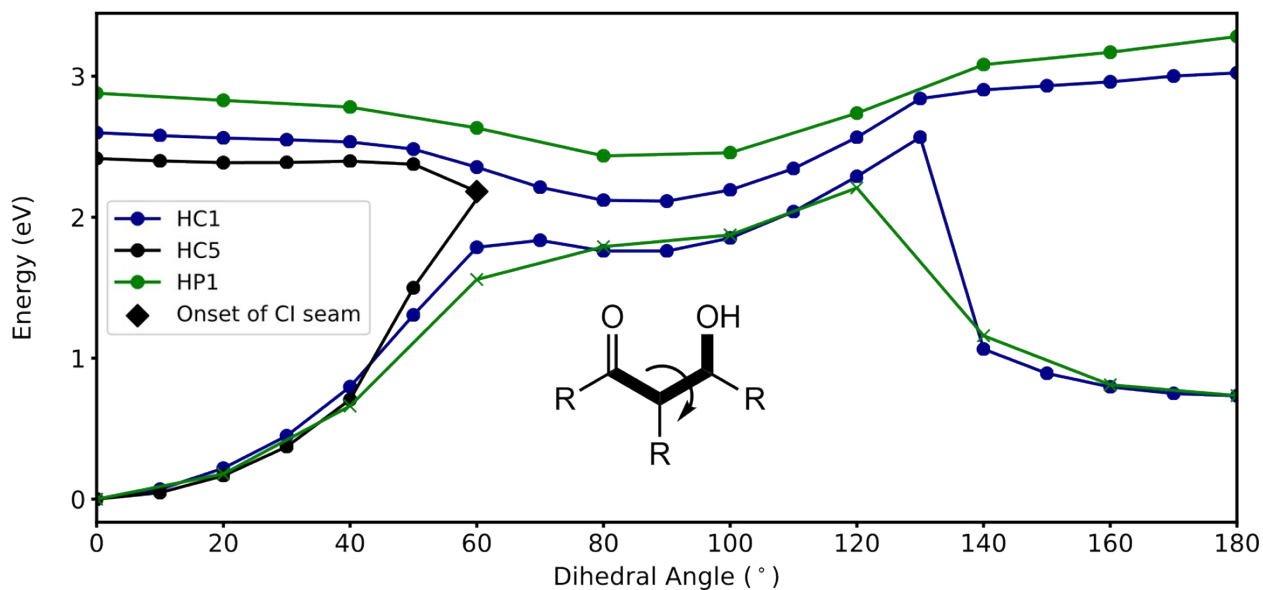

Figure S13: Relaxed geometry scan of the torsional angle (shown inset) for **HC1**, **HC5** and **HP1** in vacuum, calculated at TD-ωB87X-D/6-31G(d). For **HC5**, the scan cannot proceed further than $60°$ due to the convergence of the two electronic states.

S7   Orbitals in CASPT2 Calculations

	FC	KS$_1$	MECI

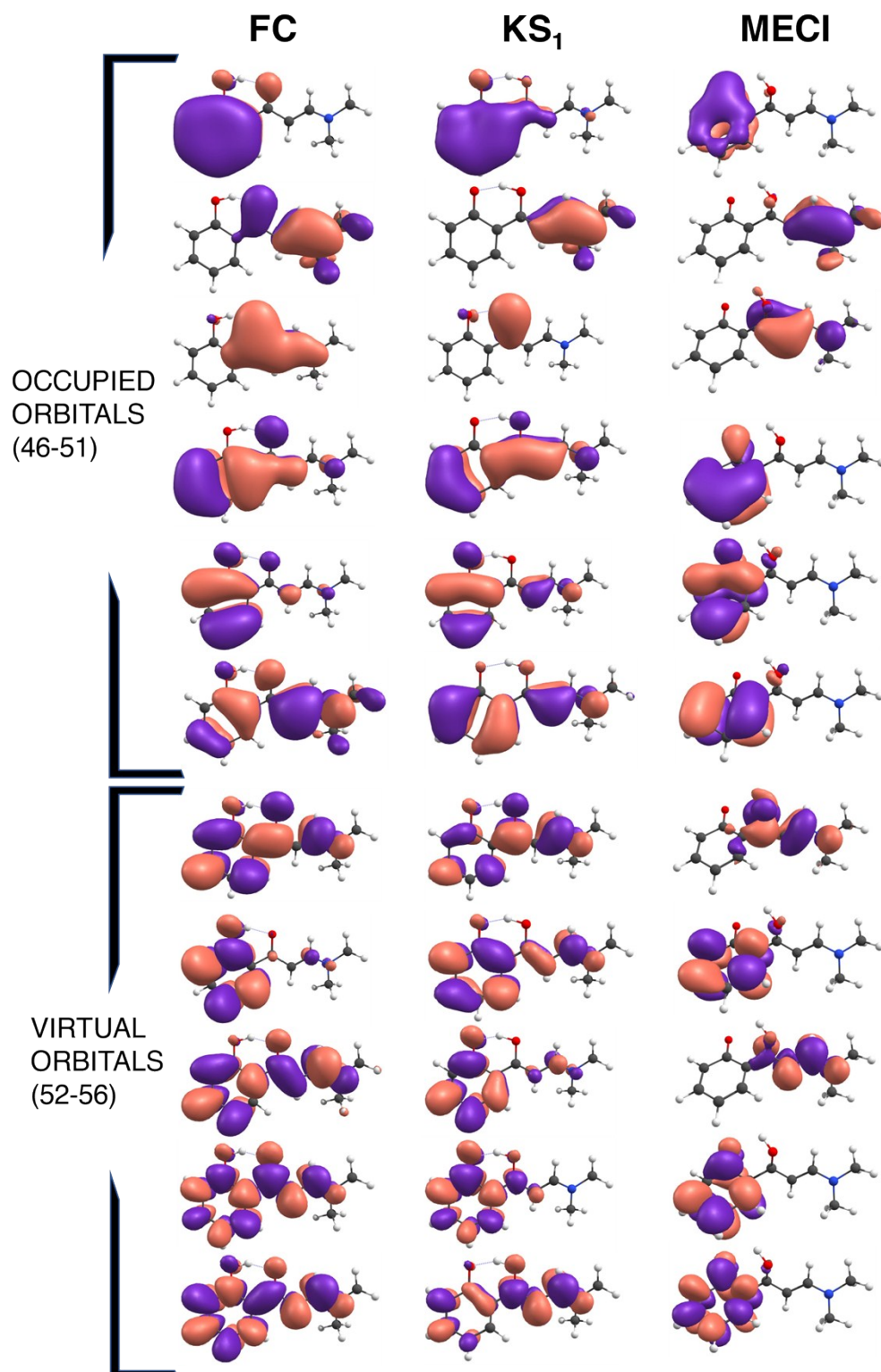**OCCUPIED ORBITALS (46-51)**

VIRTUAL ORBITALS (52-56)

Figure S14: Orbitals in the active space for the CASPT2 calculations, where the active space consists of 12 electrons in 11 orbitals. Orbitals shown for each of the Franck-Condon (FC), keto S_1 (KS$_1$) and minimum energy conical intersection (MECI) calculations.
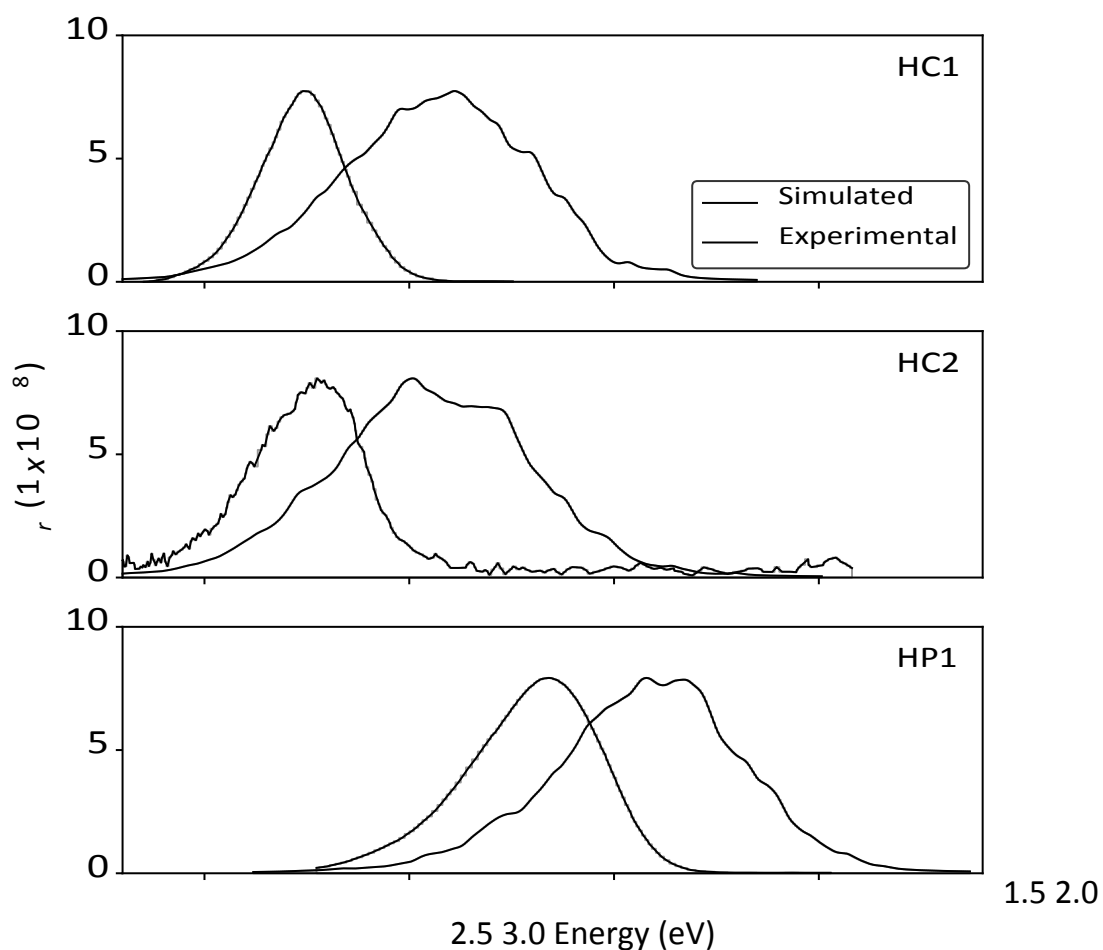
S8   Crystalline Emission Spectra

Figure S15: Emission spectra in molecular crystal for 7$\mathring{}$A clusters for **HC1**, **HC5** and **HP1**, calculated at TD-ωB97X-D/6-311++G(d,p)) in Ewald fitted point charges. Single point energies were calculated for 2000 initial conditions based upon a Wigner distribution of the excited state frequencies calculated at ONIOM(TD-ωB97X-D/6-311++G(d,p):HF/STO-3G) level with Ewald embedding. They are compared to experimental spectra for **HC1**,[5] **HC5**,[5] and **HP1**.[6]

References

(1) Kistler, K. A.; Spano, F. C.; Matsika, S. A benchmark of excitonic couplings derived from atomic transition charges. *Journal of Physical Chemistry B* **2013**, *117*, 2032–2044.

(2) Arag´o, J.; Troisi, A. Dynamics of the Excitonic Coupling in Organic Crystals. *Phys. Rev. Lett.* **2015**, *114*, 1–5.

(3) Fornari, R. P.; Arago´, J.; Troisi, A. Exciton Dynamics in Phthalocyanine Molecular Crystals. *J. Phys. Chem. C* **2016**, *120*, 7987–7996.

(4) Gierschner, J.; Varghese, S.; Park, S. Y. Organic Single Crystal Lasers: A Materials View. *Advanced Optical Materials* **2016**, *4*, 348–364.

(5) Cheng, X.; Wang, K.; Huang, S.; Zhang, H.; Zhang, H.; Wang, Y. Organic Crystals with Near-Infrared Amplified Spontaneous Emissions Based on 2-Hydroxychalcone Derivatives: Subtle Structure Modification but Great Property Change. *Angew. Chem., Int. Ed.* **2015**, *54*, 8369–8373.

(6) Tang, B.; Liu, H.; Li, F.; Wang, Y.; Zhang, H. Single-Benzene Solid Emitters with Lasing Properties Based on Aggregation-Induced Emissions. *Chem. Commun.* **2016**, *52*, 6577–6580.